IEEE Access
Multidisciplinary ⋮ Rapid Review ⋮ Open Access Journal

Received August 25, 2020, accepted September 17, 2020, date of publication September 21, 2020, date of current version October 13, 2020.

Digital Object Identifier 10.1109/ACCESS.2020.3025640

Multi-Process Integrated Planning and Guidance for Return of Reusable Aircraft Under Time Constraint

CHANG-ZHU WEI[1], ZE ZHANG[2], YUAN LI[1], AND YONGYUAN LI[3]

[1]Harbin Institute of Technology, Harbin 150001, China
[2]Beijing Institute of Control and Electronic Technology, Beijing 100038, China
[3]Research and Development Center, China Academy of Launch Technology, Beijing 100076, China

Corresponding author: Yuan Li (liyuan@stu.hit.edu.cn)

This work was supported by the Open Fund of National Defense Key Discipline Laboratory of Micro-Spacecraft Technology under Grant HIT.KLOF.MST.2018028.

ABSTRACT As the launch frequency of reusable launch vehicle (RLV) increases, the requirement of landing site management is increasing. Especially, the return flight time of RLV should be constrained to improve the utilization of landing site. In this paper, a multi-process integrated (MPI) planning and guidance algorithm for deorbit phase and reentry phase is proposed to meet the mission requirement of RLV. Firstly, the states of RLV at reentry point and deorbit point are given by MPI planning algorithm through inverse calculation. To be specific, by taking the terminal state as the initial value, the reentry point is obtained by the backward calculation based on a cosine-quadratic bank angle profile. According to the relationship among the reentry point, the deorbit time and the deorbit range, the parameters of deorbit phase can be calculated by efficient interpolation based on deorbit ability analysis. The bank angle profile is adjusted to make estimated total flight range approximate the predefined total range by particle swarm optimization algorithm. After that, guidance algorithm considering the terminal position and time constraints of the whole flight phase is given, and the trajectory optimization problem related to brake angle and start-up time is transformed into a series of convex optimization problems in deorbit phase, which can be solved by primal-dual interior-point method with better computational performance and satisfactory accuracy. In the reentry phase, the bank angle profile is designed and updated with improved predictor-corrector algorithm to correct the error during the flight. Finally, the feasibility and robustness of the propose algorithm are verified by multi-mission planning guidance simulation and Monte Carlo simulation.

INDEX TERMS RLV, time constraint, backward calculation, range estimation, convex optimization, improved predictor-corrector guidance.

I. INTRODUCTION

In recent years, reusable launch vehicles (RLVs) such as X-37B space plane, X-37C space plane and SKYLON have attracted much attention due to low cost, high degree of autonomy, rapid launch and multi-application. Compared with the first generation RLV (space shuttle), the second generation RLV has smaller size and weight, higher simplicity and higher reliability and safety. Therefore, the flight tasks undertaken by RLV are more flexible. In a mission cycle, multiple on-orbit maneuvers are required to perform different missions, where the reentry conditions and landing site differ. In addition, traditional offline planning method cannot satisfy the high frequency emission requirements of RLV high efficiency due to the higher launch frequency and shorter interval between two successive missions [1], [2]. Furthermore, the return time of RLV should approximate the predefined value for the convenience of landing site management and measurement. However, because of the complex flight environments, the planning and guidance problems under time constraint for second generation RLV are more challenging.

The return flight profile of RLV commonly comprises two phases, namely deorbit phase and reentry phase. Extensive researches on the trajectory planning and guidance problem of these two phases have been carried out in the past decades.

The associate editor coordinating the review of this manuscript and approving it for publication was Her-Terng Yau.

Some scholars have studied the minimum-energy problem and minimum-time deorbit problem in deorbit phase under impulse assumption [3]–[7]. It is easier to solve the problems under impulse assumption, but constant thrust is often used in practical engineering. Mease *et al.* [8] transformed the design of flight trajectory into the design of reference drag acceleration or drag-energy profile based on evolved acceleration guidance logic for entry (EAGLE). Wang *et al.* [9] improved the EAGLE and determined the timing of twice bank angle overturning by numerical prediction, then used the feedback linearization method to track the parameters. Lu [10] proposed a quasi equilibrium glide guidance method based on Quasi-Equilibrium glide condition (QEGC). The reentry constraint was transformed into the form of bank angle-velocity profile and altitude-velocity profile, and the secant method was used to solve the single parameter search problem. A feasible trajectory can be quickly generated, and then the linear quadratic regulator (LQR) was used to track trajectory. With the advance in processor performance, many scholars have studies the guidance algorithm based on predictor-corrector method [11]–[16]. Brunner and Lu [17] conducted a large number of simulations and found that the predictive-correction reentry guidance exhibited a good robustness even under aerodynamic deviation. Guo *et al.* [18] presented an improved predictor-corrector reentry guidance law. He converted all path constraints into overload variable constraints and obtained the required longitudinal and lateral overloads by line-of-sight guidance. A feasible flight path can be generated to guide the space vehicle to Terminal Area Energy Management (TAEM) smoothly and safely. Jiang *et al.* [19] proposed a reentry guidance method by redesigning the attack angle profile with Newton iterative method considering the situation of aircraft fault. Then the traditional predictor-corrector method was used to design the bank angle. The above-mentioned planning and guidance methods are generally designed based on terminal state such as velocity, height or range without considering time constraint.

Zhang and Li [6] proposed a velocity-to-be-gained deorbit guidance law. This algorithm can obtain velocity-to-be-gained by solving a two-body two-point boundary value problem, and then the corrected portion related to the J2 term can be calculated analytically through the state space perturbation method. It can satisfy terminal constraints on flight path angle, period and location of the reentry interface (or additional constraints) considering the J2 perturbation. Some scholars used the method of online trajectory optimization to design reference trajectory [20], [21]. Trajectory optimization can restrict any constraints including time. However, due to the high sensitivity of initial value, local convergence and high computational complexity, online optimization is difficult to be applied in engineering. Li *et al.* [22] designed a time-coordinated reentry guidance algorithm for missile based on predictive correction and designed a quadratic function type of bank angle profile. In the flight process, the parameters of the bank angle profile were modified by the method of binary Newton iteration so as to restrict terminal range and time. Fang *et al.* [23] proposed a reentry guidance method with adjustable flight time based on neural network. Firstly, the factors affecting flight time are analyzed, and the neural network is trained. In the flight process, the control parameters are adjusted by the real-time estimated flight time by neural network, and the purpose of adjusting time is realized. In recent years, convex optimization algorithm has been widely applied to solve the online trajectory planning and guidance problem [24]–[31], which is also of referential significance to this study.

The deorbit phase and reentry phase are tightly coupled, because the end of deorbit phase is the beginning of reentry phase. Therefore, the planning and guidance should be integrated for RLV's return. Motivated by the abovementioned analysis, this paper aims to develop multi-process integrated (MPI) planning and guidance algorithm under time constraint. The main contributions of this paper can be summarized as follows:

1. An MPI time-controlled planning algorithm by inverse calculation is designed for the first time. The parameters of entry point are calculated by backward calculation with cosine-quadratic bank angle profile, and the parameters of deorbit phase is given according to the deorbit ability. MPI planning algorithm comprehensively considers the whole-flight control ability and flight conditions of each flight phase, with emphasis on the ability to deorbit and the ability to glide in the atmosphere.

2. A time-controlled deorbit guidance algorithm is proposed. To ensure the accuracy of reentry point and the flight time, the optimal control problem related to brake angle and start-up time is transformed into a series of convex optimization problems in the deorbit phase, which can be solved by primal-dual interior-point method rapidly and accurately. The proposed method has better computational performance and satisfactory accuracy compared with the traditional method.

3. An improved predictor-corrector reentry guidance algorithm considering time constraint for the reentry phase is proposed. The bank angle profile is updated by predictor-corrector method to correct the deviation during the flight in real-time, which meets the requirements of altitude, velocity, time and range of TAEM interface. The nonlinear equations in predictor-corrector method are solved by convex optimization algorithm rapidly and efficiently.

The remainder of this paper is organized as follows. The problem formulation of RLV return under time constraint is given in section II. Planning and guidance algorithms for return of RLV under time constraint is given in section III. Section IV presents simulation analysis. Finally, the conclusion of this paper is provided in section V.

II. PROBLEM FORMULATION

The return flight profile of the RLV commonly comprises two phases, namely deorbit phase and reentry phase. Numerous researches on the trajectory planning and guidance problem of these two phases have been carried out in the past decades.

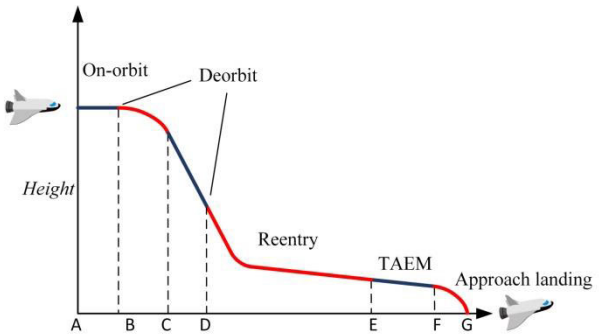

FIGURE 1. Schematic diagram of RLV return.

A. DYNAMICS MODEL DEVELOPMENT

The common reentry profile of RLV is presented in the Figure 1. The phase of AB is the on-orbit flight phase, in which the RLV is still flying in orbit at orbital velocity. The phase of BC is deorbit phase, during which the engine works continuously to change orbit. The phase of CD is the orbital transition phase, during which the RLV glides into the atmosphere without power (The terminal altitude of this phase is 120km). The phase of DE is the reentry phase. EF phase is TAEM, and FG phase is the approach landing phase [16]. This paper mainly investigates the MPI planning and guidance problem of the flight phase from A to E under time constraint.

By regarding the earth as a homogeneous rotating sphere, the exo-atmospheric dynamics of RLV can be expressed as:

$$\frac{\mathrm{d}\boldsymbol{r}}{\mathrm{d}t} = \boldsymbol{v} \tag{1}$$

$$\frac{\mathrm{d}\boldsymbol{v}}{\mathrm{d}t} = -\frac{\mu}{r^3}\boldsymbol{r} + \frac{\boldsymbol{P}}{m} \tag{2}$$

where (1) and (2) are the position vector and velocity vector of RLV, respectively. m represents the mass of RLV and $\boldsymbol{P}$ represents the engine thrust.

The atmospheric dynamics of RLV considering the rotation of the earth can be expressed as (differential w.r.t. time)

$$\dot{v} = -D - \left(\frac{\sin\gamma}{r^2}\right) + \Omega^2 r\cos\phi(\sin\gamma\cos\phi - \cos\gamma\sin\phi\cos\psi) \tag{3}$$

$$\dot{\gamma} = \frac{1}{v}[L\cos\sigma + (v^2 - \frac{1}{r})(\frac{\cos\gamma}{r}) + 2\Omega v\cos\phi\sin\psi + \Omega^2 r\cos\phi(\cos\gamma\cos\phi + \sin\gamma\cos\psi\sin\phi)] \tag{4}$$

$$\dot{\psi} = \frac{1}{v}[\frac{v^2}{r}\cos\gamma\sin\psi\tan\phi + \frac{\Omega^2 r}{\cos\gamma}\sin\psi\sin\phi\cos\phi + \frac{L\sin\sigma}{\cos\gamma} - 2\Omega v(\tan\gamma\cos\psi\cos\phi - \sin\phi)] \tag{5}$$

$$\dot{r} = v\sin\gamma \tag{6}$$

$$\dot{\theta} = \frac{v\cos\gamma\sin\psi}{r\cos\phi} \tag{7}$$

$$\dot{\phi} = \frac{v\cos\gamma\cos\psi}{r} \tag{8}$$

where r denotes the radial distance from the earth center to the RLV; λ and ϕ are longitude and latitude, respectively; v represents the velocity of RLV relative to the earth's surface; γ represents the flight path angle, which is defined as the angle between velocity vector and local horizontal level; ψ represents the heading angle, which is defined as the angle between the projection of velocity on the local horizontal plane and the local due north direction, and can be measured clockwise from the local due north; σ is the bank angle; Ω is the rate of rotation of the earth; L and D are respectively the lift acceleration and drag acceleration provided by the aerodynamic force on the RLV:

$$L = \frac{\rho v^2 S_{ref} C_L}{2m} \tag{9}$$

$$D = \frac{\rho v^2 S_{ref} C_D}{2m} \tag{10}$$

where ρ is air density at the location of the RLV; S_{ref} is the reference area of RLV; C_D and C_L are drag coefficient and lift coefficient, respectively, and both of them are determined by attack angle α, Mach number and aerodynamic shape of RLV.

Then the parameters above are nondimensionalized as follows: length is normalized by the average radius of the earth $R_0 = 6378$km; velocity is normalized by the first cosmic velocity $\sqrt{\mu/R_0}$; acceleration is normalized by the average acceleration of gravity on the earth's surface μ/R_0^2; time is normalized by $\sqrt{R_0/g_0}$.

B. MULTIPLE CONSTRAINTS

In the outer atmosphere, the time limit of BC phase is

$$T_{BC} \le T_{F\max} \tag{11}$$

where $T_{F\max}$ is the maximum running time of the engine.

In the atmosphere, the path constraints on heating rate, overload and dynamic pressure are:

$$Q = k_Q\sqrt{\rho}v^{3.15} \le Q_{\max} \tag{12}$$

$$N = \frac{\sqrt{L^2 + D^2}}{g} \le N_{\max} \tag{13}$$

$$q = \frac{\rho v^2}{2} \le q_{\max} \tag{14}$$

where k_Q is a constant related to the structure of the RLV, g is the acceleration of gravity on the RLV (take $g = 9.81$m/s). $Q_{\max}, N_{\max}$ and $q_{\max}$ are the maximum allowable heating rate, overload and dynamic pressure, respectively.

To improve the smoothness ($\dot{\gamma} = 0$) of the flight trajectory, soft constraint (quasi-equilibrium glide condition) is introduced as follows:

$$L\cos\sigma + \left(v^2 - \frac{1}{r}\right)\frac{\cos\gamma}{r} = 0 \tag{15}$$

The constraints on attack angle and bank angle are given by:

$$\alpha \le \alpha_{\max} \tag{16}$$

$$|\sigma| \le \sigma_{\max} \tag{17}$$

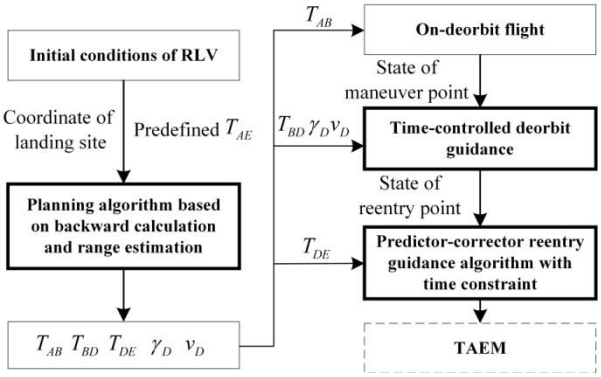

FIGURE 2. Flowchart of the proposed planning and guidance algorithm.

TAEM interface has rigorous requirements on the terminal altitude, velocity, time and remaining range, so as to ensure the stable flight of TAEM. So the terminal constraints of reentry phase are:

$$r\left(t_E\right) = r_{\text{TAEM}} \tag{18}$$

$$v\left(t_E\right) = v_{\text{TAEM}} \tag{19}$$

$$s_{togo}\left(t_E\right) = s_{togo\_\text{TAEM}} \tag{20}$$

$$t_E = t_{\text{TAEM}} \tag{21}$$

where h_{TAEM}, v_{TAEM} and t_{TAEM} are the desired initial altitude, velocity and time of TAEM, respectively. s_{togo_TAEM} is the required great-circle range to the landing site and s_{togo} is the great-circle range to the landing site in actual flight, both of which are normalized by R_0.

III. MPI PLANNING AND GUIDANCE ALGORITHM UNDER TIME CONSTRAINT

Aiming at the mission requirement of RLV returning from orbit to landing site under time constraint, a planning and guidance algorithm considering deorbit ability and aerodynamic flight characteristics of the RLV is proposed in this paper. The detailed implementation steps of the proposed scheme (shown in Figure 2) are as follows:

1. Input initial mission conditions: initial conditions of RLV (orbit parameters, engine parameters, mass characteristics and aerodynamic characteristics), flight process constraints (attack angle, bank angle, heating rate, dynamic pressure and overload constraints) and flight terminal constraints (time constraint, velocity constraint, altitude constraint and range constraint).

2. MPI planning: The time of on-orbit flight phase T_{AB} the time of orbit-change phase T_{BD}, the time of reentry phase T_{DE}, the path angle of reentry point γ_D and the velocity of reentry point v_D can be determined based on backward calculation and range estimation.

3. On-orbit flying: RLV arrives at deorbit point B from initial point A for T_{AB}.

4. MPI guidance: RLV achieves the TAEM interface E at a set time t_E^* by MPI guidance algorithm.

A. MPI PLANNING ALGORITHM UNDER TIME CONSTRAINT

Based on a comprehensive consideration of flight characteristics and flight environment in every phase, flight time of each phase and handover conditions can be determined. The MPI planning algorithm under time constraint is divided into three steps:

- Obtain reentry points by backward calculation based on a quadratic bank angle profile.
- Estimate total range based on deorbit ability and backward calculation results.
- Adjust bank angle profile to make the estimated total flight range approximate the predefined total range by particle swarm optimization algorithm (PSO).

1) OBTAIN A REENTRY POINT BY BACKWARD CALCULATION

The backward calculation is to determine an initial state according to a given terminal state by backward integration. In the backward calculation, the reentry point D is start point and reentry point (E) is ending point. The expression of backward integration using fourth-order Runge Kutta method is:

$$\begin{cases} k_1 = f\left(t_m, u_m\right) \\ k_2 = f\left(t_m - h/2, u_m - hk_1/2\right) \\ k_3 = f\left(t_m - h/2, u_m - hk_2/2\right) \\ k_4 = f\left(t_m - h/2, u_m - hk_3\right) \\ u_{m+1} = u_m - h\left(k_1 + 2k_2 + 2k_3 + k_4\right)/6 \end{cases} \tag{22}$$

If the state of point E, attack angle and bank angle are determined, the whole reentry flight can be calculated accurately according to the Eqs.(3)-(8) and (22).

The velocity and altitude of point E are set to be the same as TAEM interface. Subpoint of E is on the projection to the earth surface of AG linked line. s_{togo_TAEM} represents the range from E to G. The initial flight path angle is tuned by experience, and the direction from A to E is taken as the initial heading angle.

In the longitudinal motion, the attack angle and the bank angle profile are set in fixed form. The attack angle is designed as a piecewise function versus velocity as usual in reentry guidance:

$$\alpha = \begin{cases} \alpha_1, & v \le v_{\alpha 1} \\ \dfrac{(\alpha_2 - \alpha_1)(v - v_{\alpha 1})}{(v_{\alpha 2} - v_{\alpha 1})} + \alpha_1, & v_{\alpha 1} < v \le v_{\alpha 2} \\ \alpha_2, & v \ge v_{\alpha 2} \end{cases} \tag{23}$$

α_1, α_2, $v_{\alpha 1}$ and $v_{\alpha 2}$ are determined by considering gliding ability, thermal protection, and flight control [10].

The bank angle profile is designed in the same form which used in reentry guidance (the design of profile is explained later in this paper).

$$|\sigma\left(v\right)| = \arccos\left(av^2 + bv + c\right) \tag{24}$$

In other words, the cosine value of bank angle is a quadratic function versus velocity, as shown in Figure 3.

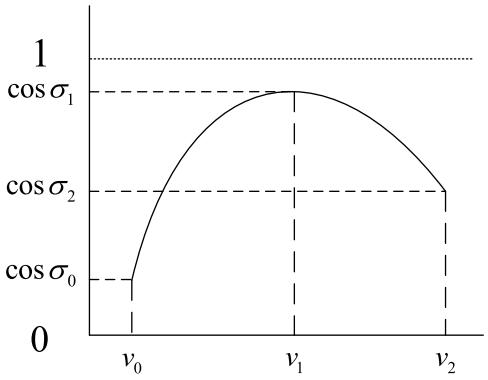

FIGURE 3. Schematic diagram of bank angle profile.

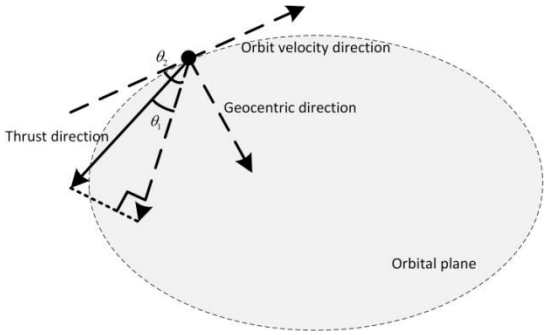

FIGURE 4. Schematic diagram of brake angle in BC phase.

where a, b, c are determined by v_0, v_1, v_2, $\cos\sigma_0$, $\cos\sigma_1$ and $\cos\sigma_2$, (25), as shown at the bottom of the page.

Set $v_0 = v_{TAEM}$. σ_0 is determined by v_{TAEM}, h_{TAEM} and Eq.(15). v_2 is set to be larger than v_0, $v_1 = (v_0 + v_2)/2$, $\sigma_1\sigma_2$ are adjustment parameters.

In lateral motion, the bank angle sign $\text{sign}(\sigma)$ is determined by the heading error corridor that is used by the space shuttle reentry guidance to limit the heading angle [23]:

$$\text{sign}(\sigma^i(v)) = \begin{cases} -1, & \Delta\psi \geq \Delta\psi_{\text{up}} \\ 1, & \Delta\psi \leq \Delta\psi_{\text{down}} \\ \text{sign}(\sigma^{i-1}(v)), & \Delta\psi_{\text{down}} \leq \Delta\psi \leq \Delta\psi_{\text{up}} \end{cases} \tag{26}$$

where $\Delta\psi$ is heading angle deviation. $\text{sign}(\sigma^{i-1}(v))$ is previous bank angle sign. $\Delta\psi_{\text{up}}$ and $\Delta\psi_{\text{down}}$ are the heading error corridor. Set $\Delta\psi_{\text{up}}$ and $\Delta\psi_{\text{down}}$ to be small constant values to keep the accuracy of heading:

$$\Delta\psi_{up} = -\Delta\psi_{down} = \psi_c \tag{27}$$

Altitude at 120km is termination criteria of backward integration. The state of reentry point $\boldsymbol{x}_D$, flight time T_{DE} and range S_{DE} are obtained after backward integration.

2) TOTAL RANGE ESTIMATION BASED ON DEORBIT ABILITY AND BACKWARD CALCULATION RESULTS

Based on deorbit ability and backward calculation results, total range can be estimated. Simplify the deorbit process to analyze deorbit ability (the relationship among state parameters of reentry points) as follows: it is considered that the attitude remains unchanged during the braking phase. Then, the deorbit process can be described by the braking angle θ_1 and θ_2 (θ_1 is the angle between thrust direction and orbit surface, and the θ_2 is the angle between the projection of the thrust on the longitudinal plane of the orbit and the tangent of the orbit) and the engine ignition time. Figure 4 shows the schematic diagram of θ_1 and θ_2.

Numerical integral of dynamic model (1) and (2) from deorbit points to reentry points is carried out by setting different combinations of θ_1, θ_2 and the engine ignition time. The relationship among state parameters of reentry points can be obtained. State parameters of accessible reentry points are shown in Figure 5 and Figure 6.

Figure 5 shows the nonlinear relationship among flight time from deorbit point to reentry point T_{BD}, path angle of reentry point γ_D and velocity v_D of reentry point. Construct a two-dimensional interpolation table $\tilde{T}_{BD}(\gamma, v)$ based on these three parameters. The strong linearity between S_{BD} and T_{BD} is shown in Figure 6. The data of S_{BD} and T_{BD} are fitted as a linear function $\tilde{S}_{BD}(T)$ by least square method.

T_{BD} can be estimated according to the interpolation table $\tilde{\boldsymbol{T}}_{BD}(\gamma, v)$, velocity v_D and path angle γ_D. In this paper, assume that the time T_{EG} from the start of TEAM to landing is fixed. So it only needs to limit time between A and E.

T_{AB} can be determined by

$$T_{AB} = T_{AE} - T_{BD} - T_{DE} \tag{28}$$

where T_{AE} is the predefined total flight time between A and E.

S_{BD} can be estimated according to T_{BD} and $\tilde{S}_{BD}(T)$. On-orbit flight range S_{AB} can be estimated according to the on-orbit flight time T_{AB}:

$$S_{AB} = T_{AB}\omega_0 \tag{29}$$

where ω_0 is orbital angular velocity.

$$\begin{aligned} a &= \frac{2\left(\cos\sigma_0 - 2\cos\sigma_1 + \cos\sigma_2\right)}{(v_0 - v_2)^2} \\ b &= \frac{\cos\sigma_0 v_0 + 3\cos\sigma_0 v_2 - 4\cos\sigma_1 v_0 - 4\cos\sigma_1 v_2 + 3\cos\sigma_2 v_0 + \cos\sigma_2 v_2}{(v_0 - v_2)^2} \\ c &= \frac{\cos\sigma_0 v_0 v_2 + \cos\sigma_0 v_2^2 - 4\cos\sigma_1 v_0 v_2 + \cos\sigma_2 v_0^2 + \cos\sigma_2 v_0 v_2}{(v_0 - v_2)^2} \end{aligned} \tag{25}$$

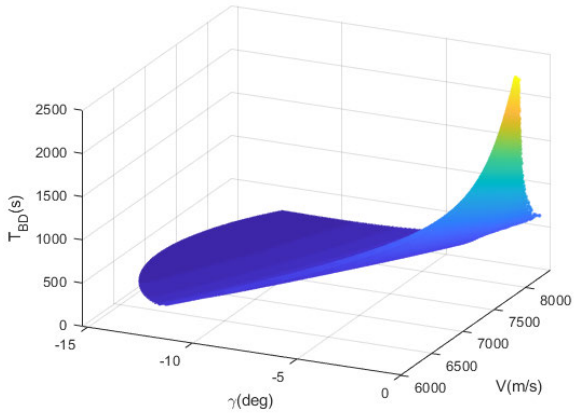

FIGURE 5. The relationship among the T_{BD}, path angle γ_D and reentry velocity v_D of reentry points.

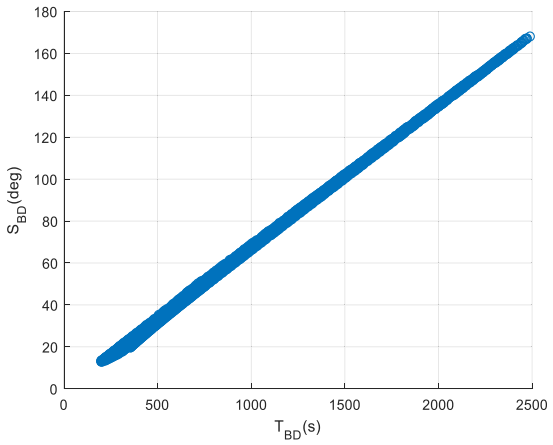

FIGURE 6. The relationship between S_{BD} and T_{BD}.

It is assumed that the landing site is located near the track of RLV's subastral point, and the total range can be estimated

$$\tilde{S}_{AE} = S_{AB} + S_{BD} + S_{DE} \tag{30}$$

3) UPDATE BANK ANGLE PROFILE BY PARTICLE SWARM OPTIMIZATION

The deviation between estimated total range and predefined total range can be corrected by adjusting bank angle profile parameters σ_1 and σ_2. The nonlinear problem P1 can be rewritten as:

$$\begin{aligned} \text{P1:}\ \ &\min \left| \tilde{S}_{AE}(\sigma_1, \sigma_2) - S_{AE} \right| \\ &\text{s.t.}\ |\sigma_1| \le \sigma_{\max} \\ &\quad |\sigma_2| \le \sigma_{\max} \end{aligned} \tag{31}$$

There is a strong non-linear relation between (σ_1, σ_2) and $\tilde{S}_{AE}$. The traditional gradient optimization method may fall into the local minimum or diverge. In this paper, PSO is applied to operate global search and obtain the optimal parameters.

When solving the optimization problem, each particle is randomly initialized in the solution space and modified based on its historical location and current best location. At each iteration, once individual extreme point and global extreme point, represented as $\boldsymbol{p}_i$ and $\boldsymbol{p}_g$, are found, particles update their velocity and position as follows:

$$\begin{aligned} \boldsymbol{v}_{id}^{k+1} &= \boldsymbol{v}_{id}^{k} + C_1 r_1 (\boldsymbol{p}_{id} - \boldsymbol{x}_{id}^{k}) + C_2 r_2 (\boldsymbol{p}_{gd} - \boldsymbol{x}_{id}^{k}) \\ \boldsymbol{v}_{id}^{k+1} &= \begin{cases} \boldsymbol{v}_d^{\max}, & \boldsymbol{v}_{id}^{k+1} \ge \boldsymbol{v}_d^{\max} \\ -\boldsymbol{v}_d^{\max}, & \boldsymbol{v}_{id}^{k+1} < \boldsymbol{v}_d^{\max} \end{cases} \\ \boldsymbol{x}_{id}^{k+1} &= \boldsymbol{x}_{id}^{k} + \boldsymbol{v}_{id}^{k+1} \end{aligned} \tag{32}$$

where $\boldsymbol{v}_{id}^{k}$ and $\boldsymbol{x}_{id}^{k}$ are the current velocity and position of the dth dimension($d = 1, 2$) for i th particle in the k th iteration, respectively. C_1 and C_2 are learning factors, r_1, r_2 are random numbers between 0 and 1.

Set termination criteria as

$$\left| \tilde{S}_{AE}(\sigma_1, \sigma_2) - S_{AE} \right| \le \delta_S \tag{33}$$

where δ_S is the permissible deviation of range.

Figure 7 is the flowchart of the proposed MPI planning under time constraint. The process of this planning algorithm as follows:

Step1: Set initial parameters of bank angle profile (σ_1^1, σ_2^1).

Step2: Obtain the relationship among flight time from deorbit point to reentry point T_{BD}, path angle of reentry point γ_D and velocity of reentry point v_D. Then the relationship between T_{BD} and S_{BD} can be obtained. Construct interpolation table $\tilde{T}_{BD}(\gamma, v)$ and fit functions $\tilde{S}_{BD}(T)$.

Step3: Obtain reentry points by backward calculation. Record the reentry range S_{DE}, path angle of reentry point γ_D, velocity of reentry point v_D and reentry flight time T_{DE}.

Step4: Estimate deorbit flight time T_{BD} by two-dimensional interpolation $\tilde{T}_{BD}(\gamma, v)$ and estimate deorbit range S_{BD} by fit functions $\tilde{S}_{BD}(T)$. Calculate on-deorbit range S_{AB} by on-orbit time T_{AB} and calculate total range $\tilde{S}_{AE}$ by adding S_{AB}, S_{BD} and S_{DE}.

Step5: If the distance between $\tilde{S}_{AE}$ and S_{AE} is close enough, finish planning with recording T_{AB}, T_{BD}, γ_D and v_D. Otherwise adjust the bank angle profile by PSO, then return to step3 and substitute σ_1^i, σ_2^i.

B. MPI GUIDANCE WITH TIME CONSTRAINT

The time-controlled planning algorithm is proposed based on the nominal condition. Considering the deviation during the flight, MPI guidance algorithm of the whole flight phase needs to be studied. In exo-atmosphere, the engine of RLV needs to turn on and the RLV leaves the orbit and reentry at expected time with high accuracy of the flight path angle, height and velocity. As for the traditional close-loop guidance algorithm, accuracy of the flight path angle and velocity cannot be ensured at the same time. With the development of the computational technology, the online trajectory optimization method has been developed rapidly, which provides an effective way to solve the guidance problem of vehicles. In this paper, a convex-optimization-based algorithm is applied to solve the guidance problem in deorbit phase of RLV.

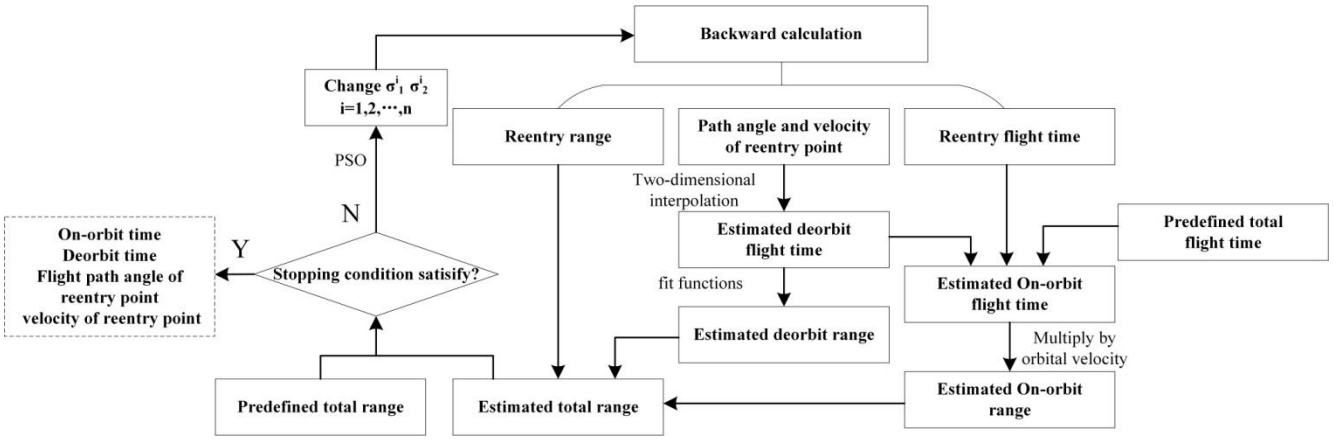

FIGURE 7. Flowchart of the proposed time-controlled planning algorithm for return of RLV.

Firstly, the terminal constraints $\boldsymbol{\varphi}$ in the deorbit phase of RLVs are the height, velocity and the flight path angle at reentry point:

$$\boldsymbol{\varphi} = \begin{bmatrix} v(t_D^*) - v^* \\ \gamma(t_D^*) - \gamma^* \\ h(t_D^*) - h^* \end{bmatrix} = 0 \tag{34}$$

The independent variable of $\boldsymbol{\varphi}$ are the direction of thrust θ_1, θ_2 and running time of the engine T_{BC}. In general, this problem is formulated as nonlinear equations, which can be solved by Newton method. However, without good initial guess, Newton method cannot solve the problem efficiently, and even divergence may be caused in some cases. To improve the computational efficiency and robustness of the algorithm, the terminal constraints are relaxed as:

$$\boldsymbol{\varphi'} = \begin{bmatrix} v(t_D^*) - v^* \\ \gamma(t_D^*) - \gamma^* \\ h(t_D^*) - h^* \end{bmatrix} - \boldsymbol{\xi} = 0 \tag{35}$$

where the relaxation variable $\boldsymbol{\xi}$ is applied. And then, the magnitude of $\boldsymbol{\xi}$ is expressed as the accuracy of the terminal constraints, which should be as small as possible. In this phase, the optimal control problem can be formulated as:

$$\min\ J = \|\boldsymbol{\xi}\| \tag{36}$$

subject to

$$\boldsymbol{\varphi'} = \boldsymbol{\varphi} - \boldsymbol{\xi} = 0 \tag{37}$$

In theory, the convex optimization problem can be solved in polynomial time with no need for initial guesses supplied by the user [32], [33]. To solve the optimal control problem rapidly and accurately, the terminal constraint should be transformed as a linear one. In this paper, Taylor expansion is applied to linearize the terminal constraint based on the solution in present iteration:

$$\boldsymbol{\varphi'}\left(\boldsymbol{x}^k\right) + \frac{\partial \boldsymbol{\varphi'}}{\partial \boldsymbol{x}^k}\Delta \boldsymbol{x} = 0 \tag{38}$$

where $\boldsymbol{x} = \begin{bmatrix} \theta_1 & \theta_2 & T_{BC} \end{bmatrix}'$ is the optimal variable.

Considering the accuracy of the linearization, the magnitude of Δx should be constrained. To decrease the complexity of the optimization problem, the magnitude of Δx is punished in the performance index. And the convex optimization problem can be formulated as:

$$\min\ J = \|\boldsymbol{\xi}\| + \alpha_x \|\Delta \boldsymbol{x}\| \tag{39}$$

subject to

$$\boldsymbol{\varphi'}\left(\boldsymbol{x}^k\right) + \frac{\partial \boldsymbol{\varphi'}}{\partial \boldsymbol{x}^k}\Delta \boldsymbol{x} = 0 \tag{40}$$

where α_x is the penalty coefficient of Δx.

The convex optimization problem Eq.(39) and Eq.(40) can be solve by the primal-dual interior-point method ∗∗ iteratively until the convergence condition is satisfied. And the optimal solution $\boldsymbol{x} = \begin{bmatrix} \theta_1 & \theta_2 & T_{BC} \end{bmatrix}'$ are the guidance command of RLV.

In atmosphere, the reentry phase can be divided into initial descent phase and gliding phase. In the initial descent phase, the RLV is flying at a maximum attack angle and zero bank angle. Quasi-equilibrium glide condition [34] is set as termination criteria.

In the gliding phase, the attack angle is designed as Eq.(23). In order to meet the terminal range-to-go and time constraints simultaneously, the bank angle magnitude profile is designed as a quadratic function of v. In addition, among all terms of the formula (4), only $L\cos\sigma$ contains σ in longitudinal motion. So bank angle profile is designed as Eq.(24). The range-to-go of the terminal moment $s_{togo}\,(t_E)$ and terminal time t_E can be regarded as implicit functions of σ_1 and σ_2, respectively. So σ_1 and σ_2 are determined by solving nonlinear equations:

$$F\,(\boldsymbol{x}) = \begin{bmatrix} f_1\,(\boldsymbol{x}) \\ f_2\,(\boldsymbol{x}) \end{bmatrix} = \begin{bmatrix} 0 \\ 0 \end{bmatrix} \tag{41}$$

where $\boldsymbol{x} = [\sigma_1, \sigma_2]'$, and the equality constraints are:

$$\begin{aligned} f_1\,(\boldsymbol{x}) &= t_E(\boldsymbol{x}) - t_{TAEM} \\ f_2\,(\boldsymbol{x}) &= s_{togo}(\boldsymbol{x}) - s_{togo\_TAEM} \end{aligned} \tag{42}$$

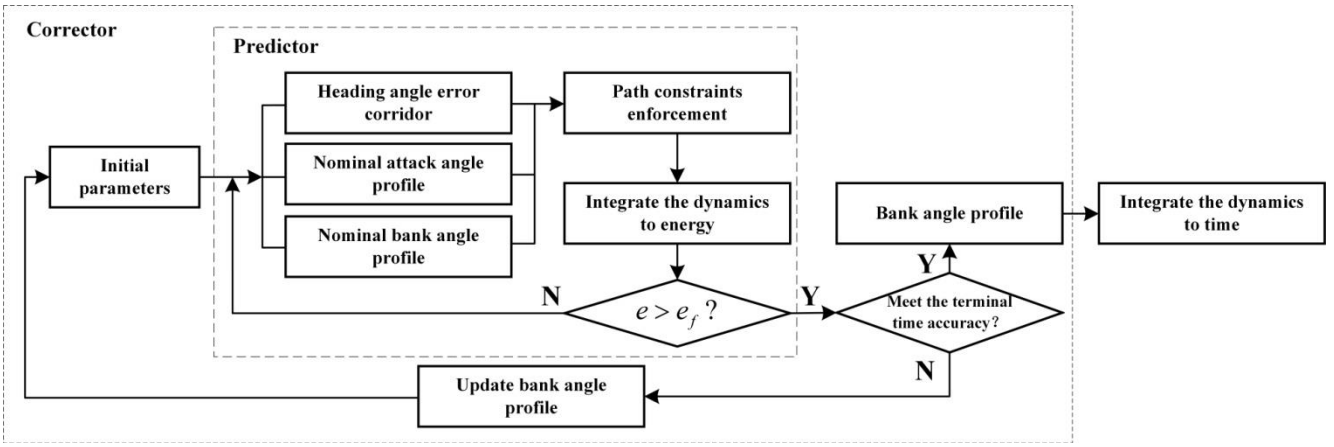

FIGURE 8. Process of the reentry guidance.

To obtain σ_1 and σ_2, the convex optimization method (same as that in Sec III.B) is utilized to solve the nonlinear equation.

Define normalized energy as:

$$e = \frac{1}{r} - \frac{v^2}{2} \tag{43}$$

The time-derivative of energy is given by:

$$\frac{\mathrm{d}e}{\mathrm{d}t} = vD \tag{44}$$

The reentry dynamics of RLV considering the rotation of the earth can be expressed as (differential w.r.t. energy)

$$\begin{aligned}\frac{\mathrm{d}v}{\mathrm{d}e} &= \frac{1}{Dv}[-D - \left(\frac{\sin\gamma}{r^2}\right) \\ &\quad + \Omega^2 r\cos\phi(\sin\gamma\cos\phi - \cos\gamma\sin\phi\cos\psi)] \quad (45)\\ \frac{\mathrm{d}\gamma}{\mathrm{d}e} &= \frac{1}{Dv^2}[L\cos\sigma + (v^2 - \frac{1}{r})(\frac{\cos\gamma}{r}) + 2\Omega v\cos\phi\sin\psi \\ &\quad + \Omega^2 r\cos\phi(\cos\gamma\cos\phi + \sin\gamma\cos\psi\sin\phi)] \quad (46)\\ \frac{\mathrm{d}\psi}{\mathrm{d}e} &= \frac{1}{Dv^2}\left[\frac{L\sin\sigma}{\cos\gamma} + \frac{v^2}{r}\cos\gamma\sin\psi\tan\phi\right. \\ &\quad - 2\Omega v(\tan\gamma\cos\psi\cos\phi - \sin\phi) \\ &\quad \left. + \frac{\Omega^2 r}{\cos\gamma}\sin\psi\sin\phi\cos\phi\right] \quad (47)\\ \frac{\mathrm{d}r}{\mathrm{d}e} &= \frac{\sin\gamma}{D} \quad (48)\\ \frac{\mathrm{d}\theta}{\mathrm{d}e} &= \frac{\cos\gamma\sin\psi}{Dr\cos\phi} \quad (49)\\ \frac{\mathrm{d}\phi}{\mathrm{d}e} &= \frac{\cos\gamma\cos\psi}{Dr} \quad (50)\\ \frac{\mathrm{d}t}{\mathrm{d}e} &= \frac{1}{Dv} \quad (51)\\ \frac{\mathrm{d}s}{\mathrm{d}e} &= -\frac{\cos(\psi - \psi_{ref})\cos\gamma}{Dr} \quad (52)\end{aligned}$$

where ψ_{ref} is the azimuth of landing site.

Integrate Eqs. (45)-(52), and the terminal condition is satisfied with:

$$e_f = \frac{1}{r_{TAEM}} - \frac{v_{TEAM}^2}{2} \tag{53}$$

$F(\boldsymbol{x})$ can be calculated as follows:

$$t_E(\boldsymbol{x}) = t(e_f) \tag{54}$$

$$s_{togo}(\boldsymbol{x}) = s(e_f) \tag{55}$$

where the bank angle sign is determined by the Eq.(24), and heading error corridor function versus velocity is shown as follow:

$$\begin{aligned}\Delta\psi_{up} &= -\Delta\psi_{down} \\ &= \begin{cases}\psi_1, & v \le v_{\psi 1} \\ \frac{(\psi_2-\psi_1)(v-v_{\psi 1})}{(v_{\psi 2}-v_{\psi 1})} + \psi_1, & v_{\psi 1} < v \le v_{\psi 2} \\ \psi_2, & v \ge v_{\psi 2}\end{cases} \quad (56)\end{aligned}$$

where ψ_1, ψ_2, $v_{\psi 1}$ and $v_{\psi 2}$ are determined by considering gliding ability and mission requirements.

The predictor-corrector guidance process is shown in Figure 8 and detailed implementation steps are as follows:

Step1. In the guidance period, the current state of RLV is taken as the initial value. Then integrate Eqs.(45)∼(52) to predict the terminal state ($e = e_f$) based on the bank angle magnitude profile in Eq.(24) and attack angle magnitude profile in Eq.(23). The sign of bank angle is controlled by heading angle error corridor in Eq.(26).

Step2. σ_1 and σ_2 are updated by convex optimization with the terminal remaining range deviation and terminal time deviation as constraints. When the deviation is small enough to meet the requirement, the iteration is finished and the bank angle profile are obtained.

Step3. Receding-horizon strategy is used during the flight. In other words, the bank angle profile is applied until the new guidance command is calculated and updated in next guidance cycle.

TABLE 1. Initial orbit elements.

Orbital parameters	Value
orbit semi-major axis	6678km
orbit inclination	45°
orbit eccentricity	0
longitude of ascending node	0°
argument of perigee	0°
True anomaly	-45°

TABLE 2. Expected reentry point status.

reentry point state	γ_D (°)	v_D (m/s)	T_{BD} (s)
Value	-5.9	7635.0	354.0

IV. SIMULATION RESULTS AND ANALYSIS

In this section, the performance of proposed MPI planning and guidance algorithm under time constraint is verified through a series of simulations, including planning simulation, trajectory generation simulation and guidance simulation.

A. SIMULATION CASES DESCRIPTION

The initial mass of RLV is set to 1000kg and the mass of the fuel is set to 400kg. The constant thrust of the engine is set to 8000N, and the maximum running time of the engine is set to190s. The reference area is set to $2m^2$. The initial orbit elements of RLV are as follows:

The bank angle is constrained with the range of $-90° \leq \sigma \leq 90°$. The permissible deviation of range is set to $\delta_S = 150$km. In addition, the desired terminal range-to-go is set to 150km, terminal height is set to 28km, terminal velocity is set to 1000m/s.

All the numerical results shown below are generated using a computer with Intel i5-9400 processor (2.9 GHz, 6 cores, 6 threads), 16.0 GB memory and Win10 system. The simulation environment is Microsoft Visual Studio 2015, and the development language is C++.

B. MPI RETURN PLANNING AND TRAJECTORY GENERATION SIMULATIONS

Firstly, the feasibility and superiority of proposed algorithm are verified by a deorbit trajectory generation based on convex optimization. Then the performance of MPI planning algorithm is verified by a whole process planning and trajectory generation simulation.

1) The initial parameters of deorbit phase are as shown in Tab.1, and the expected terminal parameters of deorbit phase are shown in Tab.2. The deorbit problem is solved by proposed convex optimization and traditional Newton method. The convex optimization problems are solved by the MOSEK software.

The simulation results of Newton method and Convex optimization are shown in Figure 9∼Figure 13. Tab.3 is the comparison of two algorithms in deorbit phase. It can be

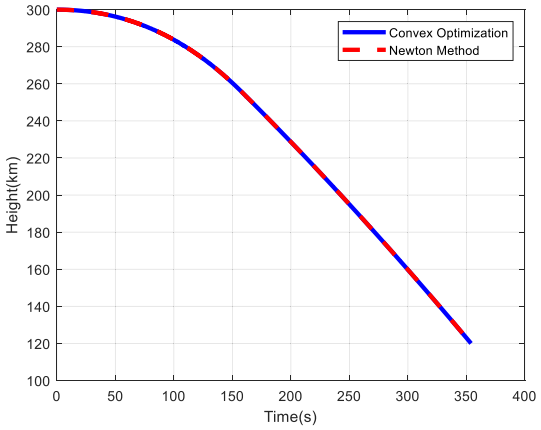

FIGURE 9. Time history of height.

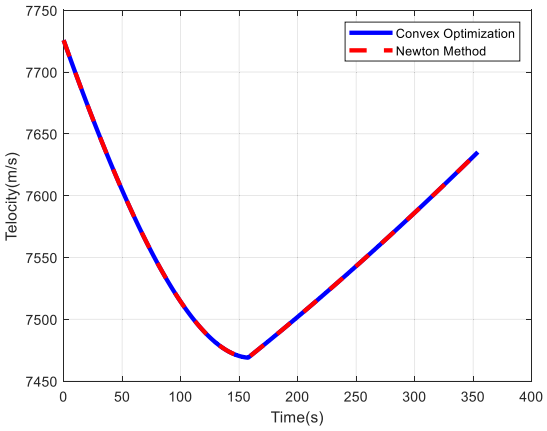

FIGURE 10. Time history of velocity.

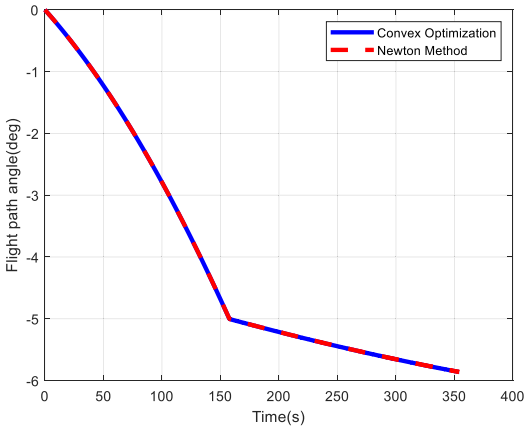

FIGURE 11. Time history of path angle.

seen that the optimal solutions obtained by both methods are very similar, and the guidance commands of both algorithms are very similar, too. This verifies the accuracy and validity of the algorithm proposed in this paper. However, without good initial guess, it takes 23 iterations and 17.1s for Newton method to converge to the expected solution. Under the same condition, the average CPU time of the proposed algorithm is 0.21s, and it only takes 7 iterations and 1.47s to solve

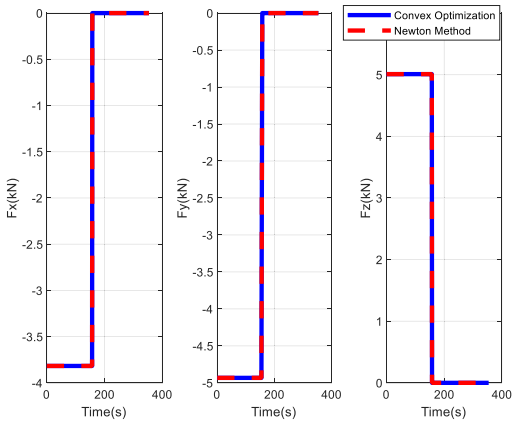

FIGURE 12. Time history of engine thrust direction.

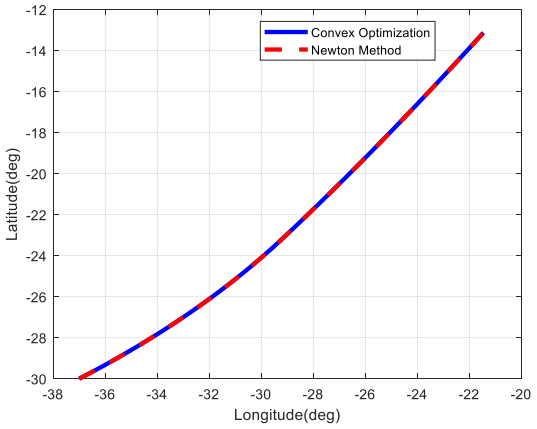

FIGURE 13. Ground tracks.

TABLE 3. Comparison of two algorithms in deorbit phase.

Terminal error	γ_D (°)	v_D (m/s)	T_{BD} (s)	CPU time (s)
Newton method	0.0001	0.21	0.01	17.1
Convex optimization	-0.0002	0.18	-0.01	1.47

the problem, so there is enough time for the on-orbit RLV to calculate the solution. In addition, the algorithm based on convex optimization can solve the optimal control problem with fewer iterations without the requirement of good initial guess, which proves the excellent robustness and computational performance of the proposed algorithm. In conclusion, the algorithm proposed in this paper has excellent computational efficiency and robustness, and can compute the guidance command rapidly, which has great application prospect in onboard computation of guidance command.

2) In this part, two return missions with different landing points are designed to verify the performance of proposed MPI planning algorithm. The initial parameters of deorbit phase are shown in Tab.1. Tab.4 shows two different return missions under time constraint.

TABLE 4. Position of landing sites and time constraint.

Missions	Longitude (°)	Latitude (°)	Time constraint (s)
Mission1	5	18	1250
Mission2	53	14	1900

TABLE 5. Parameters of attack angle profile and heading error corridor.

Parameters	Value
α_1	11.5°
α_2	20.0°
$v_{\alpha 1}$	1000m/s
$v_{\alpha 2}$	7000m/s
σ_0	56.06°
v_0	1000m/s
v_1	4000m/s
v_2	7000m/s
ψ_c	1°
ψ_1	5°
ψ_2	15°
$v_{\psi 1}$	1000m/s
$v_{\psi 2}$	5000m/s

TABLE 6. Initial state of backward calculation.

	θ (°)	ϕ (°)	ψ (°)	γ (°)	v (m/s)	h (km)
Mission1	4.10	16.97	36.80	-6	1000	28
Mission2	51.76	13.39	51.76	-6	1000	28

TABLE 7. Time of each phase.

Missions	T_{AB} (s)	T_{BC} (s)	T_{BD} (s)	T_{DE} (s)
Mission1	172.20	157.70	181.48	738.97
Mission2	456.94	171.11	176.73	1095.93

The parameters of attack angle profile and heading error corridor are shown in Tab.5.

According to the initial position and terminal state, the initial state of backward calculation is set as Tab.6.

Planning for return of RLV under time constraint can be completed according to the analysis of backward calculation and deorbit ability of RLV, as shown in Figure 5 and Figure 6. Tab.7 shows the reference flight time of each phase by planning algorithm.

The simulation results under nominal conditions are shown in Figure 14∼Figure 27. Figure 14 and Figure 15 show the time history of height in different missions; Figure 16 and Figure 17 show the time history of velocity in different

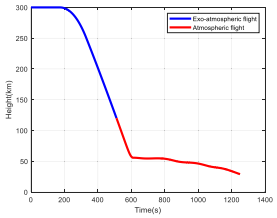

FIGURE 14. Time history of height in mission1.

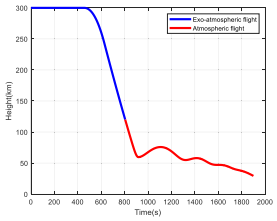

FIGURE 15. Time history of height in mission2.

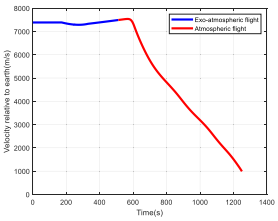

FIGURE 16. Time history of velocity in mission1.

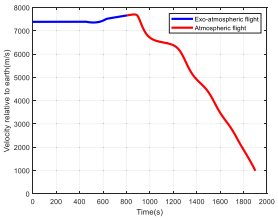

FIGURE 17. Time history of velocity in mission2.

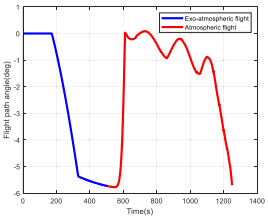

FIGURE 18. Time history of flight path angle in mission1.

missions. Figure 18 and Figure 19 show the time history of flight path angle in different missions. Figure 20 and Figure 21 show the ground track in different missions. Figure 22 and Figure 23 show the engine thrust direction in exo-atmospheric flight in different missions. Figure 24 and Figure 25 show the time history of bank angle in atmospheric flight in different missions. Figure 26 and Figure 27 show the time history of attack angle in atmospheric flight indifferent missions.

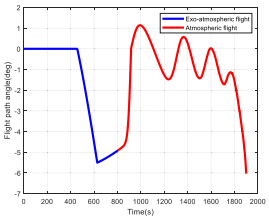

FIGURE 19. Time history of flight path angle in mission2.

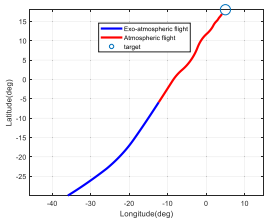

FIGURE 20. Ground track in mission1.

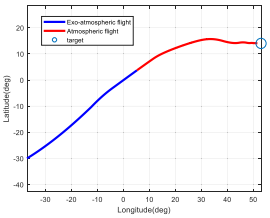

FIGURE 21. Ground track in mission2.

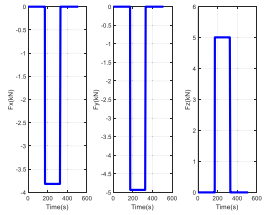

FIGURE 22. Engine thrust direction in mission1.

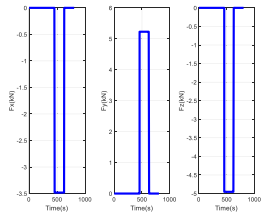

FIGURE 23. Engine thrust direction in mission2.

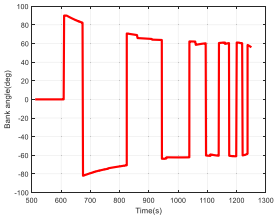

FIGURE 24. Bank angle in mission1.

It can be seen from Tab.8 that the proposed planning and guidance algorithm can successfully guide RLV to enter

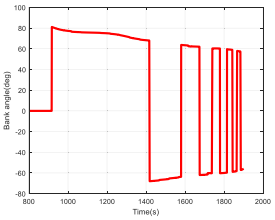

FIGURE 25. Bank angle in mission2.

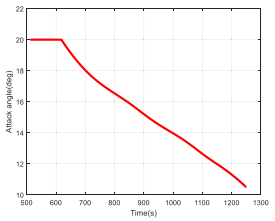

FIGURE 26. Attack angle in mission1.

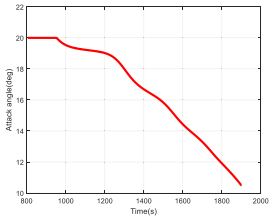

FIGURE 27. Attack angle in mission2.

TABLE 8. Terminal state errors in nominal cases.

height (km)	velocity (m/s)	range-to-go (km)	Time (s)
0.95	-9.25	1.44	0.35
1.31	-12.81	2.59	0.71

TABLE 9. The perturbation settings in Monte Carlo simulation.

Disturbance parameters	Δv_0	$\Delta \psi_0$	$\Delta \theta_0$	$\Delta \phi_0$
Value	$\pm$100m/s	$\pm 1^\circ$	$\pm 2^\circ$	$\pm 2^\circ$

Disturbance parameters	ΔC_L	ΔC_D	ρ	P
Value	$\pm$10%	$\pm$10%	$\pm$10%	$\pm$3%

TAEM by meeting the conditions of velocity, height, range-to-go and time. Therefore, the feasibility of the proposed planning and guidance algorithm in the RLV return problem is verified based on the above simulation results.

C. MPI RETURN GUIDANCE SIMULATIONS

To verify the robustness of the guidance algorithm in the deorbit and reentry phase, the deviation shown in Tab. 9 is introduced to carry out 200-run Monte Carlo deorbit-reentry guidance simulations based on mission 2 by considering the disturbance of initial velocity, initial heading, initial longitude, initial latitude, engine thrust and aerodynamic coefficients.

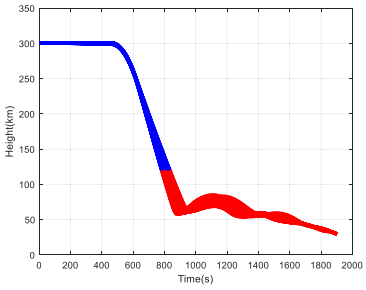

FIGURE 28. Curve of height.

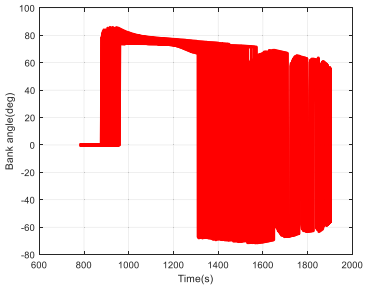

FIGURE 29. Curve of bank angle.

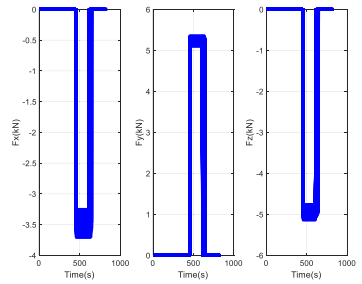

FIGURE 30. Curve of thrust direction.

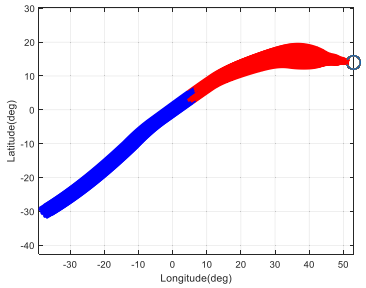

FIGURE 31. Curve of ground tracks.

The simulation results under deviation conditions are shown in Figure 28∼Figure 33. Figure 28 shows the time history of height. Figure 29 shows the time history of velocity. Figure 30 shows engine thrust direction in exo-atmospheric. Figure 31 shows curve of bank angle in atmospheric flight. Figure 32 shows the dispersion of terminal time error and terminal range error. Figure 33 shows the dispersion of terminal velocity error and terminal height error.

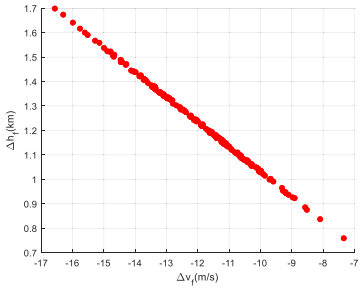

FIGURE 32. Terminal error of velocity-height.

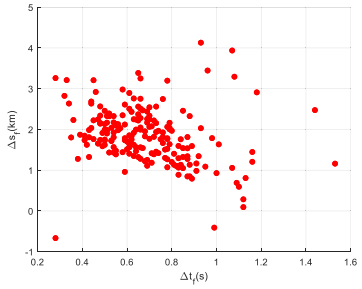

FIGURE 33. Terminal error of time-range.

TABLE 10. Statistical results for mission2 in deviation cases.

Terminal state errors	Δh_f	Δv_f	Δt_f	Δs_f
Best	0.76km	-7.34 m/s	0.28s	0.09km
Worst	1.70km	-16.57m/s	1.53s	4.13km
mean	1.23km	-12.00m/s	0.69	1.84km
3σ	0.52km	5.11m/s	0.61s	2.04km

There is a linear relationship between terminal velocity error and terminal height error in Figure 33, because energy is termination criteria of reentry phase.

Tab.10 shows the statistical results of 100-run Monte Carlo simulations. The worst Δh_f is 1.65km, the worst Δv_f is -16.06m/s, the worst Δt_f is 1.73s and the worst Δt_f is 3.12km. It can be seen that the proposed algorithm can successfully guide the RLV to TAEM with acceptable accuracy.

The Monte Carlo simulation results show that the proposed algorithm has excellent adaptability and robustness, and can provide guidance for return of RLV under time constraint.

V. CONCLUSION

In this paper, by comprehensively considering the ability and feature of each flight phase, a planning and guidance integration algorithm for RLV considering time constraint is proposed. Firstly, a time-constrained planning algorithm is proposed through inverse calculation to obtain the time of each phase and parameters of reentry point. The state of entry point is given by backward calculation with a cosine-quadratic bank angle profile, and the parameters of deorbit phase is given according to the control ability. Then, a time-constrained deorbit guidance algorithm is applied to meet the requirement of reentry. Then the problem of solving the nonlinear equations in the deorbit phase is transformed into an optimization problem, which can be solved online by convex optimization method. The proposed algorithm has faster computation speed than traditional Newton method. Next, a predictor-corrector reentry guidance algorithm with time constraint is given. The bank angle profile is designed, in which the cosine value of bank angle is regarded as a quadratic function versus velocity. Moreover, the bank angle profile is updated by convex optimization method. The guidance under time constraint is completed by updating the bank angle profile in longitudinal motion and designing heading error corridor in lateral motion Finally, the results of two planning return planning simulation and Monte Carlo guidance simulation show that the proposed algorithm has excellent robustness, feasibility and application value in engineering.

REFERENCES

[1] M. Benton, J. Berry, and H. Benner, "2nd generaton RLV: Overview of concept development process and results," in *Proc. AIAA/ICAS Int. Air Space Symp. Expo., Next*, vol. 100, 2003, pp. 1–7.

[2] K. Sivan and S. Pandian, "An overview of reusable launch vehicle technology demonstrator," *Curr. Sci*, vol. 114, pp. 38–47, Jan. 2018.

[3] B. A. Galman, "Erratum: Minimum energy deorbit," *J. Spacecraft Rockets*, vol. 3, no. 7, pp. 1030–10336, 1966.

[4] J. M. Baker, B. E. Baxter, and P. D. Arthur, "Optimum deboost altitude for specified atmospheric entry angle," *AIAA J.*, vol. 1, no. 7, pp. 1663–1665, Jul. 1963.

[5] M. C. Baldwin and P. Lu, "Optimal deorbit guidance," *J. Guid., Control, Dyn.*, vol. 35, no. 1, pp. 93–103, Jan. 2012.

[6] H. Zhang and B. Li, "Velocity-to-be-gained deorbit guidance law using state space perturbation method," *J. Aerosp. Eng.*, vol. 31, no. 2, Mar. 2018, Art. no. 04017099.

[7] G. Chen, P. Cai, Y. Wang, L. Zhang, and J. Liang, "Trajectory optimization for asteroid landing considering gravitational orbit-attitude coupling," *IEEE Access*, vol. 7, pp. 126464–126478, 2019.

[8] K. Mease, D. Chen, S. Tandon, D. Young, and S. Kim, "A three-dimensional predictive entry guidance approach," in *Proc. AIAA Guid., Navigat., Control Conf. Exhib.*, 2000, p. 3959.

[9] S. H. Wang, L. F. Pan, X. X. Liu, and B. Zhang, "A new evolved acceleration reentry guidance for reusable launch vehicles," *Appl. Mech. Mater.*, vols. 380–384, pp. 576–580, Aug. 2013.

[10] P. Lu, "Entry guidance: A unified method," *J. Guid. Control Dyn.*, vol. 37, no. 3, pp. 713–728, 2014.

[11] M. Li and J. Hu, "An approach and landing guidance design for reusable launch vehicle based on adaptive predictor–corrector technique," *Aerosp. Sci. Technol.*, vol. 75, pp. 13–23, Apr. 2018.

[12] M. Li and J. Hu, "The comparative study of Mars entry phase's guidance methods," in *Proc. Chin. Intell. Automat. Conf.*, 2017, pp. 491–500.

[13] B. Tian, W. Fan, and Q. Zong, "Integrated guidance and control for reusable launch vehicle in reentry phase," *Nonlinear Dyn.*, vol. 80, nos. 1–2, pp. 397–412, Apr. 2015.

[14] Y. Enmi, W. Qian, K. He, and D. Di, "Accurate predictor–corrector skip entry guidance for low lift-to-drag ratio spacecraft," *Prog. Flight Dyn., Guid., Navigat., Control*, vol. 10, no. 10, pp. 105–120, 2018.

[15] X. Jiang, "Robust optimization of Mars entry trajectory under uncertainty," in *Proc. Space Flight Mech. Meeting*, Jan. 2018, p. 0721.

[16] L. Mu, X. Yu, Y. M. Zhang, P. Li, and X. Wang, "Onboard guidance system design for reusable launch vehicles in the terminal area energy management phase," *Acta Astronautica*, vol. 143, pp. 62–75, Feb. 2018.

[17] C. W. Brunner and P. Lu, "Comparison of fully numerical predictor-corrector and Apollo skip entry guidance algorithms," *J. Astron. Sci.*, vol. 59, no. 3, pp. 517–540, Sep. 2012.

[18] X. Guo, R. Qi, and X. Yao, "Predictor-corrector guidance for reentry hypersonic vehicle based on feedback linearization," in *Proc. 29th Chin. Control Decis. Conf. (CCDC)*, Chongqing, China, May 2017, pp. 6516–6521, doi: 10.1109/CCDC.2017.7978346.

[19] Y. M. Bin Jiang and R. Qi, "Fault-tolerant guidance for hypersonic vehicle based on predictor-corrector strategy," *IFAC-PapersOnLine*, vol. 50, no. 1, pp. 5244–5249, Jul. 2017.
[20] Z. Li, C. Hu, C. Ding, G. Liu, and B. He, "Stochastic gradient particle swarm optimization based entry trajectory rapid planning for hypersonic glide vehicles," *Aerosp. Sci. Technol.*, vol. 76, pp. 176–186, May 2018.
[21] D. Chai, Y.-W. Fang, Y.-L. Wu, and S.-H. Xu, "Boost-skipping trajectory optimization for air-breathing hypersonic missile," *Aerosp. Sci. Technol.*, vol. 46, pp. 506–513, Oct. 2015.
[22] Z. Li, B. He, M. Wang, H. Lin, and X. An, "Time-coordination entry guidance for multi-hypersonic vehicles," *Aerosp. Sci. Technol.*, vol. 89, pp. 123–135, Jun. 2019.
[23] K. Fang, Q. Zhang, N. I. Kun, L. Cheng, and Y. Huang, "Time-coordinated reentry guidance law for hypersonic vehicle," *Acta Aeronaut. Astronaut. Sin.*, vol. 39, no. 5, pp. 1–16, 2018.
[24] Y. Li, Y. Guan, C. Wei, and R. Hu, "Optimal control of ascent trajectory for launch vehicles: A convex approach," *IEEE Access*, vol. 7, pp. 186491–186498, 2019.
[25] Y. Ling, Y. Zhou, and Q. Luo, "Lévy flight trajectory-based whale optimization algorithm for global optimization," *IEEE Access*, vol. 5, pp. 6168–6186, 2017.
[26] J. Zheng, J. Chang, S. Yang, X. Hao, and D. Yu, "Trajectory optimization for a TBCC-powered supersonic vehicle with transition thrust pinch," *Aerosp. Sci. Technol.*, vol. 84, pp. 214–222, Jan. 2019.
[27] J. Wang, N. Cui, and C. Wei, "Optimal rocket landing guidance using convex optimization and model predictive control," *J. Guid., Control, Dyn.*, vol. 42, no. 5, pp. 1078–1092, May 2019.
[28] Z. Wang and M. J. Grant, "Minimum-fuel low-thrust transfers for spacecraft: A convex approach," *IEEE Trans. Aerosp. Electron. Syst.*, vol. 54, no. 5, pp. 2274–2290, Oct. 2018.
[29] Z. Wang and M. J. Grant, "Autonomous entry guidance for hypersonic vehicles by convex optimization," *J. Spacecraft Rockets*, vol. 55, no. 4, pp. 993–1006, Jul. 2018.
[30] J. Wang and N. Cui, "A pseudospectral-convex optimization algorithm for rocket landing guidance," in *Proc. AIAA Guid., Navigat., Control Conf.*, Jan. 2018, p. 1871.
[31] M. Sagliano, "Pseudospectral convex optimization for powered descent and landing," *J. Guid., Control, Dyn.*, vol. 41, no. 2, pp. 320–334, Feb. 2018.
[32] X. Liu, "Autonomous trajectory planning by convex optimization," Ph.D. dissertation, Iowa State Univ., Ames, IA, USA, 2013.
[33] J. F. Sturm, "Implementation of interior point methods for mixed semidefinite and second order cone optimization problems," *Optim. Methods Softw.*, vol. 17, no. 6, pp. 1105–1154, Jan. 2002.
[34] Z. Shen and P. Lu, "On-board entry trajectory planning expanded to sub-orbital flight," in *Proc. AIAA Guid., Navigat., Control Conf. Exhibit*, Aug. 2003, p. 5736.

CHANG-ZHU WEI received the B.S. degree in flight vehicle design and engineering and the Ph.D. degree in aeronautical and astronautical science and technology from the Harbin Institute of Technology, Harbin, China, in 2005 and 2010, respectively.

From 2013 to 2015, he was an Assistant Professor with the School of Astronautics, Harbin Institute of Technology, where he has been an Associate Professor since 2016. He is the author of one book, more than 30 articles, and two inventions. His research interests include advanced guidance and control methods of flight vehicle, trajectory design, and optimization of flight vehicle.

ZE ZHANG received the B.S. degree in flight vehicle design and engineering and the M.S. degree in aeronautical and astronautical science and technology from the Harbin Institute of Technology, Harbin, China, in 2018 and 2020, respectively. Since 2020, he has been with the Beijing Institute of Control and Electronic Technology. His research interests include guidance and control methods of hypersonic vehicle.

YUAN LI received the B.S. degree in flight vehicle design and engineering from the Harbin Institute of Technology, Harbin, China, in 2015, where he is currently pursuing the Ph.D. degree in aeronautical and astronautical science and technology. His research interests include advanced guidance and control methods of flight vehicle, convex optimization theory and application, and robust control and application.

YONGYUAN LI received the Ph.D. degree in flight vehicle design and engineering from the Beijing Institute of Technology, Beijing, China, in 2012. His research interests include advanced trajectory design and online planning methods of flight vehicle.